Chapter 6

Control of Single-Phase and Three-Phase DC/AC Converters

Ariya Sangwongwanich*, Ahmed Abdelhakim†, Yongheng Yang* and Keliang Zhou‡
*Aalborg University, Aalborg, Denmark, †University of Padova, Padua, Italy, ‡University of Glasgow, Glasgow, United Kingdom

6.1 INTRODUCTION

Power electronic converters have been widely used in industrial and residential applications to enable proper, reliable, and efficient power control between the source and the load. There are several types of power conversion systems categorized by the combination of sources and load types (DC or AC), as also being discussed in previous chapters of this book. Among other power conversion systems, the DC/AC converters are one of the mainstream power conditioning systems, which cover a wide range of applications, since most of the industrial loads are AC (e.g., motor drives and the utility grid). For instance, the DC/AC converters are commonly employed in motor drive systems to improve the conversion efficiency and to enable a variable speed operation [1–3]. In that case, the control target of the DC/AC converters is to regulate the motor torque and speed, and the frequency of the AC output voltage should be fully controllable.

In the last decade, the DC/AC power converters have also been widely adopted in renewable energy applications as an adaptor to the grid. For instance, in wind turbine (WT) and photovoltaic (PV) systems, the DC/AC converters are employed as a grid-side converter to transfer the extracted power from renewable sources to the AC grid [4–7]. The main objective of the grid-side DC/AC converter is to deliver the active power to the grid with a satisfied power quality, e.g., total harmonic distortion level according to the grid requirements [8]. Additionally, grid support functionalities such as reactive power injection or active power control capabilities have also been imposed in grid regulations along with the continuously increasing penetration of grid-connected WT and PV systems [9–13]. These stringent requirements are demanded in order to avoid the adverse impacts from the intermittent power injection from the

Control of Power Electronic Converters and Systems. https://doi.org/10.1016/B978-0-12-805245-7.00006-8

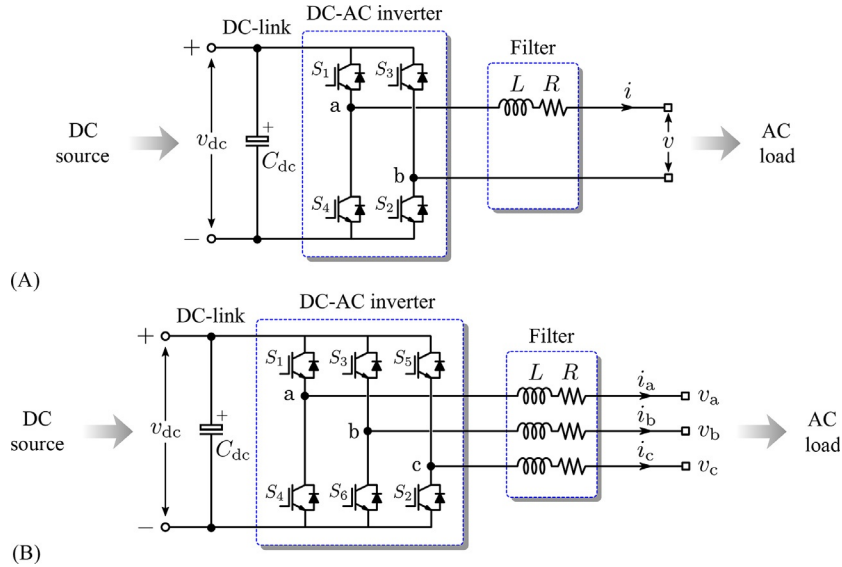

FIG. 6.1 Circuit diagram of DC/AC converters with an *L* filter to smoothen the current from the switching (*R* is its internal resistance): (A) single-phase and (B) three-phase, where C_{dc} is the DC-link capacitor.

renewables. Therefore, the control of the DC/AC converter plays an important role in achieving the above requirements and ensuring a high-performance power conversion from DC to AC.

In this chapter, the control of DC/AC converters will be discussed in details for both single- and three-phase systems. Here, the most common single- and three-phase DC/AC converters shown in Fig. 6.1 are considered. The model of the DC/AC power converter will be introduced to represent the system control dynamics. Then, the control of the three-phase DC/AC converter in the *dq*-reference frame with proportional integral (PI) controllers will be discussed, including the current controller, DC-link voltage controller, and active power and reactive power controller (also referred to as *PQ* controller). The design of each controller will be demonstrated and verified with case studies.

6.2 MODELING OF DC/AC CONVERTERS

In this part, the modeling of DC/AC converters will be provided in detail. The reference frame transformation will be first discussed, where the AC control variables (e.g., voltages and currents) will be transformed into two DC quantities through the Clarke and Park transformations. This is applied to both single- and three-phase systems. Afterward, system modeling of DC/AC converters with an *L* filter, including the current controller, the *PQ* controller, and the DC-link voltage controller will be elaborated.

6.2.1 Reference Frame Transformation

6.2.1.1 Three-Phase to the Stationary Reference Frame (abc → αβ)

Fig. 6.1B shows the circuit diagram of a three-phase, two-level DC/AC converter. As seen, there are two pairs of AC variables (voltages: v_a, v_b, v_c and currents: i_a, i_b, i_c), which are time varying according to the dynamics of each individual phase. From the modeling perspective, the mathematical model of such a system can be complicated. However, considering a balanced three-phase system, it can be represented by a two-phase system on the stationary reference frame (i.e., the $\alpha\beta$-reference frame) as

$$\begin{bmatrix} x_\alpha \\ x_\beta \end{bmatrix} = \frac{2}{3} \begin{bmatrix} 1 & -\frac{1}{2} & -\frac{1}{2} \\ 0 & \frac{\sqrt{3}}{2} & -\frac{\sqrt{3}}{2} \end{bmatrix} \begin{bmatrix} x_a \\ x_b \\ x_c \end{bmatrix} \tag{6.1}$$

where x_a, x_b, and x_c represent the voltages or currents of the system and x_α, x_β are variables on the $\alpha\beta$-reference frame. In practice, the transformation from the abc-reference frame to the $\alpha\beta$-reference frame is also called the Clarke transformation.

6.2.1.2 Stationary Reference Frame to the Synchronous Reference Frame (αβ → dq)

By applying the Clarke transformation in Eq. (6.1), the control variables (x_a, x_b, and x_c) in any balanced three-phase system are reduced to two components (x_α, x_β). Nevertheless, the $\alpha\beta$ components are still AC variables rotating at the same speed (denoted as ω) of the original three-phase AC variables. In that case, the control design is not straightforward, and the well-known proportional integral (PI) controllers cannot achieve zero-error tracking of the $\alpha\beta$ components [14]. Thus, the Park transformation ($\alpha\beta \rightarrow dq$) is applied to the $\alpha\beta$ variables, and also it gives two variables on the synchronous reference frame (i.e., the dq-reference frame) as

$$\begin{bmatrix} x_d \\ x_q \end{bmatrix} = \begin{bmatrix} \cos\theta & \sin\theta \\ -\sin\theta & \cos\theta \end{bmatrix} \begin{bmatrix} x_\alpha \\ x_\beta \end{bmatrix} \tag{6.2}$$

in which x_d, x_q are the components on the dq-reference frame and $\theta = \omega t$ is the angular position or phase with ω being the frequency. When the Park transformation in Eq. (6.2) is adopted, the two orthogonal variables on the $\alpha\beta$-reference frame will become two DC quantities on the dq-reference frame. This is usually preferable in the control design, e.g., of PI controllers.

Notably, the Park transformation can also be employed in single-phase systems. In that case, an orthogonal signal generator (OSG) is required to create a fictitious component (i.e., x_β) in-quadrature with the original variable (i.e., x_α). There are several OSG systems, which has been discussed in Ref. [5]. Once the

orthogonal variables on the $\alpha\beta$-reference frame, i.e., x_α and x_β, are obtained, the transformation to the dq-reference frame in Eq. (6.2) can be applied, similar to that for three-phase systems.

6.2.2 System Modeling

A system diagram of the two-level three-phase DC/AC converter is illustrated in Fig. 6.2, where a cascaded-control loop is employed. At the outer control loop, the active and reactive power is controlled either directly by a PQ controller (as shown in Fig. 6.2) or indirectly through the DC-link voltage regulation [15]. This is mainly determined by applications. For instance, for grid-connected photovoltaic systems, where a DC-DC stage is usually employed to optimize the power extraction, the DC-link voltage control is usually taken as the outer loop. Nevertheless, the inner control loop is generally to control the current injected to the AC load. Herein, the objective is to regulate the output current according to the reference set by the outer control loop, as demonstrated in Fig. 6.2. An output voltage reference (i.e., v_{inv}^*) of the DC/AC converter is obtained from the current controller with an inverse Park and Clark transformation. The voltage reference

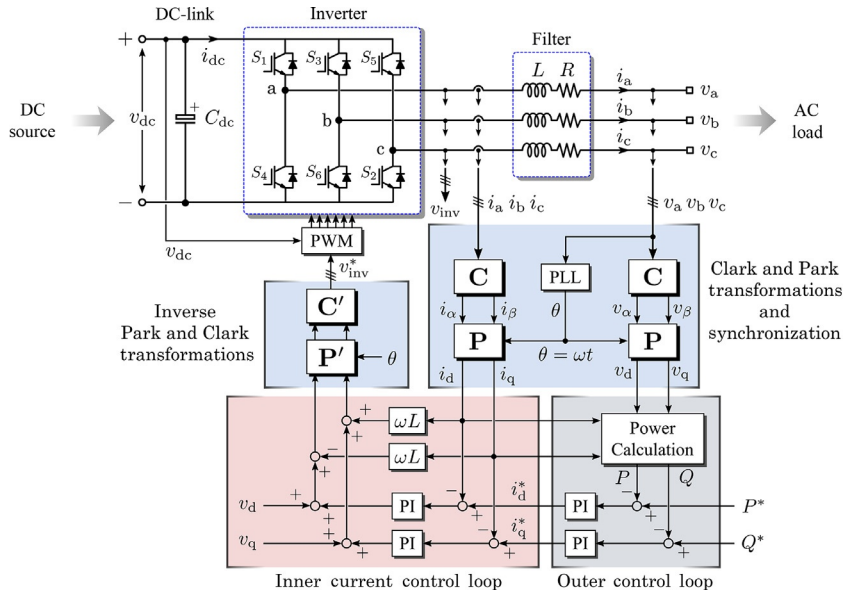

FIG. 6.2 System diagram of the DC/AC two-level converter with a cascaded-control loop in the synchronous (dq) reference frame (PLL—phase locked loop; PWM—pulse width modulation), where $\mathbf{C}, \mathbf{P}$ represents the Clark and Park transformation with $\mathbf{C}', \mathbf{P}'$ being the corresponding inverse transformation, respectively, and $\theta = \omega t$ is the phase of the output voltage with ω being the frequency. The outer control loop is a power control loop, which is able to control both active power P and reactive power Q. The subscript represents the variable on the corresponding reference frame. In certain applications, the frequency ω is assigned arbitrarily, where the PLL unit may not be necessary.

is then used for the pulse-width modulation (PWM) in order to synthesize the corresponding output voltage v_{inv} by switching the DC/AC converter. This closes the entire DC to AC power processing. Notably, a phase-locked loop (PLL) as the synchronization unit is required for the reference frame transformation to keep synchronizing with the grid. However, in certain applications, the frequency ω can be assigned arbitrarily, where the PLL may be absent. Nevertheless, the entire system should be modeled in order to design proper controllers for the DC/AC power conversion as shown in Fig. 6.2. Hereafter, the mathematical model of the entire system is derived in terms of the modeling for the current control loop, the power loop, and the DC-link.

6.2.2.1 Modeling of the Current Control Loop

The main aim of the current controller is to regulate the converter output current by generating a proper output voltage reference. Following the circuit diagram in Fig. 6.1, according to the Kirchhoff's law, the DC/AC converter output current (i.e., the current injected to the load) can be expressed in the single-phase reference frame as

$$L\frac{di}{dt} + Ri = v_1 - v \tag{6.3}$$

in which L and R are the inductance and the resistance of the filter, v_1, i, and v are the converter output voltage, the current injected to the load, and the load voltage.

Similarly, according to Figs. 6.1 and 6.2, the DC/AC converter output currents for the three-phase system can be expressed as

$$\begin{cases} L\dfrac{di_{\text{a}}}{dt} + Ri_{\text{a}} = v_{\text{a1}} - v_{\text{a}} \\ L\dfrac{di_{\text{b}}}{dt} + Ri_{\text{b}} = v_{\text{b1}} - v_{\text{b}} \\ L\dfrac{di_{\text{c}}}{dt} + Ri_{\text{c}} = v_{\text{c1}} - v_{\text{c}} \end{cases} \tag{6.4}$$

in which v_{p1}, i_p, and v_p are the converter output voltage, the current injected to the load, and the load voltage, with $p = a, b, c$ being the phase index. Applying the reference frame transformations in Eqs. (6.1), (6.2) to the three-phase model results in

$$\begin{cases} L\dfrac{di_d}{dt} + Ri_d - \omega Li_q = v_{d1} - v_d \\ L\dfrac{di_q}{dt} + Ri_q + \omega Li_d = v_{q1} - v_q \end{cases} \tag{6.5}$$

where i_d and i_q are the currents injected to the load on the dq-reference frame, v_{d1} and v_{q1} are the converter output voltages on the d- and q-axis, v_d and v_q are the load voltages on the d- and q-axis, respectively, and ω is the frequency of the system.

As discussed previously in Section 6.2.1, in the case of single-phase systems, a fictitious component (i.e., x_β) in-quadrature with the original variable (i.e., x_α) should be generated from the OSG system before applying the reference frame transformation. Afterward, the transformation to the dq-reference frame in Eq. (6.2) can be applied to Eq. (6.3) and the fictitious system, resulting in a similar system model as in Eq. (6.5). Seen from this viewpoint, the system model in the dq-reference frame is similar for both single- and three-phase systems.

It is clearly seen in Eq. (6.5) that the injected AC current can be controlled by regulating the output voltage of the DC/AC converter. However, the d- and q-axis output currents are coupled to each other, leading to a slightly complicated system from the control perspective. In addition, the load voltage also has an influence on the control dynamics. Therefore, the output voltage references (i.e., v_{d1}^* and v_{q1}^*) are modified by means of adding one decoupling term and one feed-forward voltage as

$$\begin{cases} v_{d1}^* = v_{d1} + \omega L i_q - v_d \\ v_{q1}^* = v_{q1} - \omega L i_d - v_q \end{cases} \tag{6.6}$$

The current control loop model after the modification can then be rewritten as

$$\begin{cases} L\dfrac{di_d}{dt} + Ri_d = v_{d1}^* \\ L\dfrac{di_q}{dt} + Ri_q = v_{q1}^* \end{cases} \tag{6.7}$$

in which the d- and q-axis output currents (i.e., the current injected to the load) are decoupled, as shown in Fig. 6.3. Moreover, as it is shown in Eq. (6.7), the d- and q-axis output current expressions are identical. Thus, the analysis on one axis is sufficient, as they share the same dynamics. Accordingly, the plant transfer functions from the converter output voltage references to the output current currents can be obtained as [16]

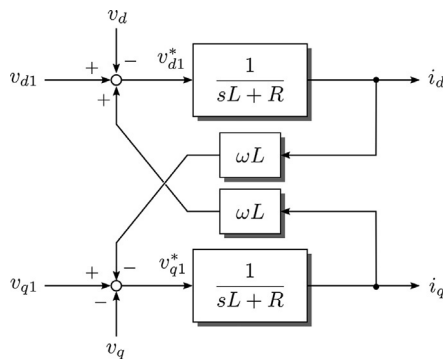

FIG. 6.3 Block diagram representation of the AC side system of three-phase DC/AC inverters in the dq-reference frame.

$$\frac{i_d(s)}{v_{d1}^*(s)} = \frac{i_q(s)}{v_{q1}^*(s)} = \frac{1}{Ls+R} \tag{6.8}$$

also indicating that the d- and q-axis output currents have the same dynamics.

6.2.2.2 Modeling of the PQ Control Loop

The concept of the PQ control (i.e., the outer control loop in Fig. 6.2) is based on the *instantaneous power theory* proposed by Akagi [17]. In the synchronous dq-reference frame, the instantaneous active power P and reactive power Q can be calculated as

$$\begin{cases} P = \frac{3}{2}\left(v_d i_d + v_q i_q\right) \\ Q = \frac{3}{2}\left(v_q i_d - v_d i_q\right) \end{cases} \tag{6.9}$$

Assuming that the PLL is aligned with the load voltage vector to the d-axis of the dq-reference frame (i.e., $v_q = 0$), the transfer functions from the d- and q-axis output currents to the active and reactive power can be calculated as

$$\frac{P(s)}{i_d(s)} = \frac{3}{2}v_d(s) = \frac{3}{2}V_m \tag{6.10}$$

$$\frac{Q(s)}{i_q(s)} = -\frac{3}{2}v_d(s) = -\frac{3}{2}V_m \tag{6.11}$$

which are simply proportional gains with V_m being the amplitude of the output load voltage. It can be noticed from Eqs. (6.10), (6.11) that, in theory, an open-loop control is sufficient to regulate the active and reactive power (assuming an ideal converter). However, a closed-loop control is practically employed to improve the control performance due to uncertainties in the system (e.g., load voltage variations and power losses), as demonstrated in Fig. 6.2.

6.2.2.3 Modeling of the DC-Link Control Loop

One alternative to control the output power of the DC/AC power converter is through the regulation of the DC-link voltage [15]. Maintaining the DC-link voltage constant (at the nominal value) ensures that all the extracted power from the DC source can be delivered to the AC load. This control scheme is widely used in photovoltaic (PV) systems, where the input power is continuously fed by the PV arrays. In addition, in the case of back-to-back power conversion systems, the (average) DC-link voltage is also commonly controlled at a desired level. This is also to ensure a proper power injection to the load, e.g., the DC-link voltage has to be at least higher than the peak grid voltage in the case of grid-connected applications.

Assuming a loss-less DC/AC power converter, the input DC power and the output active power should be balanced according to the instantaneous power theory. In that case, it gives

$$\overbrace{v_{\mathrm{dc}} C_{\mathrm{dc}} \frac{dv_{\mathrm{dc}}}{dt}}^{\text{DC input power}} = \overbrace{\frac{3}{2}\left(v_d i_d + v_q i_q\right)}^{\text{Output active power}} \tag{6.12}$$

where C_{dc} is the DC-link capacitance as shown in Fig. 6.2 and i_{dc} is the output current of the DC source. If the d-axis of the dq-reference frame is aligned with the load voltage vector (by the PLL), the q-axis component of the grid voltage becomes zero (i.e., $v_q = 0$). Applying the small-signal analysis to Eq. (6.12) can linearize the model. By doing so, the transfer function of the DC-link from the output d-axis current to the DC-link voltage can be simplified as

$$\frac{v_{\mathrm{dc}}(s)}{i_d(s)} = \frac{3}{2}\frac{V_m}{V_{\mathrm{dc}} C_{\mathrm{dc}} s} \tag{6.13}$$

with V_{dc} and I_{dc} being the average voltage and current of the DC source.

It should be noted that, although the model in Eq. (6.13) shows the control of the d-axis current through the regulation of the DC-link voltage, a reactive power injection is still possible if required. In that case, the reactive power can separately be controlled following Eq. (6.11) to generate the q-axis current reference. The decoupling of the two currents on the dq-reference frame also ensures the individual control.

6.3 CONTROLLER DESIGN

As previously mentioned, classical PI controllers are commonly used in current-controlled DC/AC converters [18,19]. This is also depicted in Fig. 6.2, in which the three-phase DC/AC converter is controlled as a current source in order to track a certain current reference in the synchronous dq-reference frame. The d- and q-axis current references (i_d^* and i_q^*) can be injected directly or calculated from the desired active and reactive power. In this case, the d-axis current i_d^* is determined by the desired active power P as shown in Eq. (6.10), while the q-axis current i_q^* is obtained from the set-point of the reactive power Q according to Eq. (6.11). Notably, an outer power loop can be employed in order to regulate the active and reactive power, as exemplified in Fig. 6.2. It is also worth mentioning that the open-loop case is sufficient in most applications.

On the other hand, the outer control loop can also be realized by the DC-link voltage regulation, which generates the d-axis reference current i_d^* [19]. This control scheme is widely used in grid-connected application, e.g., PV applications. In some cases, e.g., single-phase system, current controllers in the stationary reference frame (or corresponding to the abc-reference frame) become more attractive with a simpler control structure due to the absence of reference frame transformations. This will be further discussed in the following section.

Because of the cascaded control structure shown in Fig. 6.2, the controller design can be challenging due to possible dynamic interactions between different controllers. As a result, it is of importance to properly design the current and the DC-link voltage controllers in order to ensure a high-control performance and proper operation of the DC/AC converters. In practice, the response of the inner control loop, i.e., the current controller, should be designed to be much faster than the response of the outer control loop, i.e., the DC-link voltage controller [19]. Notably, the analysis is based on the previously discussed models in the s-domain with an assumption that the controller sampling rate is fast enough and the impact from discretization can be neglected. Accordingly, this section focuses on the design procedure of the current-controlled DC/AC converter, where the next subsections will cover the design steps of the current and DC-link voltage controllers.

6.3.1 Current Controller

According to the prior system modeling, the inner current control loops for the d- and q-axis components have the same dynamics, as implied in Eq. (6.8). Hence, the design procedure can be demonstrated only on the d-axis (i.e., for the d-axis current i_d) as shown in Fig. 6.4, in which $G_{\mathrm{PI}}^{d}(s), G_{\mathrm{delay}}(s)$, and $G_f(s)$ represent the d-component PI current controller, the elapsed delay due to the PWM and computations in the control system, and the filter (plant) transfer function.

The controller design for the q-axis current can be achieved following the same method. Nevertheless, these transfer functions in Fig. 6.4 can be given as

$$G_{\mathrm{PI}}^{d}(s) = k_{pd} + \frac{k_{id}}{s} = \frac{k_{pd}(1 + T_{id}s)}{T_{id}s} \tag{6.14}$$

$$G_{\mathrm{delay}}(s) = \frac{1}{1 + 1.5T_s s} \tag{6.15}$$

$$G_f(s) = \frac{1}{R + Ls} = \frac{T_f}{L(1 + T_f s)} \tag{6.16}$$

in which k_{pd} and k_{id} are the proportional and the integral gains of the PI current controller, $T_{id} = k_{pd}/k_{id}$ is the integrator time constant, T_s is the sampling time,

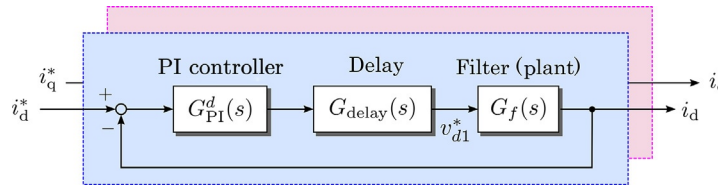

FIG. 6.4 Current control loops in the synchronous dq-reference frame, where the cross-coupling and the feed-forward terms are neglected.

L is the inductance of the employed filter, R is the equivalent series resistance of the inductor L, and $T_f = L/R$ is the filter time constant.

As shown in Fig. 6.4, the cross-coupling ($\omega L i_q$) and the voltage feed-forward (v_d) terms for the d-axis current component control loop are neglected. In that case, the two terms are considered as disturbances in the system. Accordingly, the open-loop transfer function can be expressed as

$$G_{ol}^{d}(s) = G_{\mathrm{PI}}^{d}(s) \cdot G_{\mathrm{delay}}(s) \cdot G_f(s) = \frac{k_{pd} T_f (1 + T_{id} s)}{T_{id} L s (1 + 1.5 T_s s)(1 + T_f s)} \tag{6.17}$$

Hence, the closed-loop transfer function is obtained as

$$G_{cl}^{d}(s) = \frac{G_{ol}^{d}(s)}{1 + G_{ol}^{d}(s)} = \frac{k_{pd} T_f (1 + T_{id} s)}{T_{id} L s (1 + 1.5 T_s s)(1 + T_f s) + k_{pd} T_f (1 + T_{id} s)} \tag{6.18}$$

which is also applicable for the q-axis current.

In order to analytically design the parameters of the PI current controller, the closed-loop transfer function shown in Eq. (6.18) can be simplified by choosing the integrator time constant T_{id} to be equal to the filter time constant T_f. By doing so, the closed-loop transfer function can be expressed as

$$G_{cl}^{d}(s) = \frac{k_{pd}}{L s (1 + 1.5 T_s s) + k_{pd}} = \frac{\dfrac{2k_{pd}}{3T_s L}}{s^2 + \dfrac{2}{3T_s} s + \dfrac{2k_{pd}}{3T_s L}} \tag{6.19}$$

being a typical second-order system with

$$\omega_n^2 = \frac{2k_{pd}}{3T_s L} \quad \text{and} \quad 2\zeta\omega_n = \frac{2}{3T_s} \tag{6.20}$$

where ω_n is the natural frequency and ζ is the damping ratio.

In practice, $\zeta = 1/\sqrt{2}$ is designed for an optimally damped system, which will result in an overshoot of 5% for a step response [5]. As a consequence, the proportional and integral gains can be obtained as

$$k_{pd} = \frac{L}{3T_s} \quad \text{and} \quad k_{id} = \frac{L}{3T_s T_f} \tag{6.21}$$

Finally, with the assumption that the current control loop is optimally designed, the closed-loop transfer function can then be approximated by as

$$G_{cl}^{d}(s) \approx \frac{1}{1 + 3T_s s} = \frac{1}{1 + \tau s} \tag{6.22}$$

from which the bandwidth can be estimated as

$$f_{bw}^{d} \approx \frac{1}{2\pi\tau} = \frac{1}{6\pi T_s}. \tag{6.23}$$

On the other hand, the PI controller can be tuned using MATLAB, where an interesting tool called "*pidTuner*" can be used. Using this tool, the parameters of the PI controller can be selected by importing the plant and the delay transfer functions, i.e., $G_f(s)$ and $G_{\text{delay}}(s)$, and then tuning the PI controller according to the desired bandwidth or the response time and the phase margin or the transient behavior (e.g., the rise time).

In some applications, e.g., single-phase PV systems, the DC/AC converter is normally required to operate with a unity power factor. In that case, the reference output current of the DC/AC converter is one single sinusoidal time-varying signal following the phase of the grid voltage. As discussed previously, PI controllers can be employed in the dq-reference frame. However, this can increase control complexity in terms of reference frame transformations. An alternative solution to regulate the AC signal is to use a proportional-resonant (PR) controller in the $\alpha\beta$-reference frame [20], which has a controllability of the AC signal at a specific frequency ω, e.g., the grid fundamental frequency. The transfer function of the PR controller is given as

$$G_{\text{PR}}(s) = k_{pr} + \frac{k_{ir}s}{s^2 + \omega^2} \tag{6.24}$$

in which k_{pr} and k_{ir} are the proportional and the integral gains, respectively.

From the transfer function in Eq. (6.24), the PR controller has an infinite gain at a particularly tuned frequency ω, making it capable of tracking an AC signal. The proportional gain k_{pr} can be selected in the similar way as in Eq. (6.21), while the integral gain k_{ir} is recommended as

$$k_{ir} = 2\alpha_h k_{pr} \tag{6.25}$$

where α_h is the resonant bandwidth, which should be much lower than the current controller bandwidth (e.g., $\alpha_h \ll 2\pi f_{bw}^{d}$).

In some cases, the PR controller has its implementation advantage due to the absence of the reference frame transformation. However, the ideal PR controller in Eq. (6.24) is sensitive to even a small frequency variation (which is typical grid-connected applications), leading to stability issues [20]. To address those, the nonideal PR controller can be employed in practice, whose transfer function is given as

$$G_{\text{PR}}(s) = k_{pr} + \frac{k_{ir}\omega_c s}{s^2 + 2\omega_c s + \omega^2} \tag{6.26}$$

where ω_c is the cut-off frequency that can be used to adjust the selectivity of the tracking frequency with the trade-off of the controller gain. It is recommended in Ref. [21] that the cut-off frequency ω_c should be selected in the range of 5–15 rad/s. More detailed analysis and design procedure can be found in Refs. [20–24].

6.3.2 DC-Link Voltage Controller

It has been illustrated in previous sections that the DC-link voltage can be controlled for the inner d-axis current control loop. That is, the DC-link voltage controller represents an outer loop to generate the reference for the d-axis current. This is depicted in Fig. 6.5, in which $G_{\mathrm{PI}}^{v}(s), G_v(s)$ represents the DC-link voltage PI controller and the plant (i.e., the DC-link voltage model), respectively. The transfer functions can be given as

$$G_{\mathrm{PI}}^{v}(s) = k_{pv} + \frac{k_{iv}}{s} = \frac{k_{pv}(1 + T_{iv}s)}{T_{iv}s} \tag{6.27}$$

$$G_v(s) = \frac{3}{2}\frac{V_m}{V_{\mathrm{dc}}C_{\mathrm{dc}}s} \tag{6.28}$$

where k_{pv} and k_{iv} are the proportional and the integral terms of the DC-link voltage controller, respectively, and T_{iv} is the integrator time constant. In the case of grid-connected applications, the DC-link voltage V_{dc} should be higher than the minimum required DC-link voltage, in order to allow the current controllability and avoid the over modulation, which can be determined as

- $V_{\mathrm{dc}} \geq V_m$ for single-phase systems
- $V_{\mathrm{dc}} \geq \sqrt{3}V_m$ for three-phase systems with space vector modulation (SVM) scheme
- $V_{\mathrm{dc}} \geq 2V_m$ for three-phase systems with a sinusoidal PWM scheme (SPWM)

On the other hand, the average DC-link voltage V_{dc} should not be much higher than $\sqrt{3}V_m$ when using the SVM scheme in order to avoid to high power losses.

From Fig. 6.5, the open loop transfer function of the DC-link voltage control loop can be expressed by

$$G_{ol}^{v}(s) = G_{\mathrm{PI}}^{v}(s) \cdot G_{cl}^{d}(s) \cdot G_v(s) \tag{6.29}$$

With the simplified current control loop in Eq. (6.22), the transfer function in Eq. (6.29) is given as

$$G_{ol}^{v}(s) \approx \frac{3V_m k_{pv}(1 + T_{iv}s)}{2T_{iv}V_{\mathrm{dc}}C_{\mathrm{dc}}s^2(1 + 3T_s s)} \tag{6.30}$$

Then, the phase crossover frequency ω_c can be expressed as

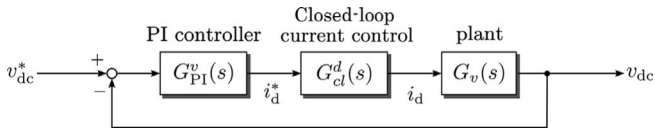

FIG. 6.5 Block diagram of the DC-link voltage control loop.

$$\omega_c = \frac{1}{\sqrt{3T_s T_{iv}}} \tag{6.31}$$

Hence, the control parameters k_{pv} and k_{iv} at the phase crossover frequency (ω_{pc}) are given by

$$k_{pv} = \frac{C_{dc}}{2\sqrt{T_s T_{iv}}} \quad \text{and} \quad k_{iv} = \frac{C_{dc}}{2\sqrt{T_s T_{iv}^3}} \tag{6.32}$$

Similarly, the PI controller can be tuned using the "*pidTuner*" in MATLAB, where the plant transfer function and the exact closed-loop transfer function of the *d*-axis current (i.e., $G_{cl}^{d}(s) \cdot G_v(s)$) can be imported. The parameters can be obtained according to the desired bandwidth or the response time, the phase margin, or the transient behavior of the system.

6.3.3 Case Study

In order to show a numerical example for the previously discussed design procedure, the controllers of a 10-kW grid-connected boost converter-fed three-phase DC/AC converter are designed in this subsection. The schematic and the entire control are shown in Fig. 6.6, and the system parameters of the double-stage DC/AC system are shown in Table 6.1. Notably, the case study

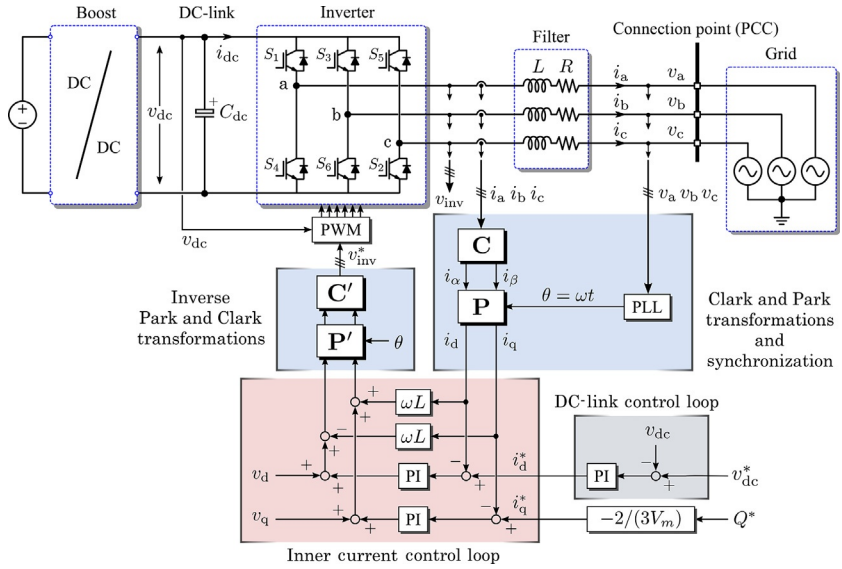

FIG. 6.6 Control structure of the DC/AC stage in a double-stage three-phase grid-connected system in the synchronous reference frame, where the outer control loop is a voltage control and the reactive power can be directly controlled and V_m is the grid phase voltage amplitude. The PLL is used for reference transformations.

TABLE 6.1 System Parameters of the 10-kW Grid-Connected Three-Phase DC/AC Converter

Parameter	Symbol	Value
DC-link voltage reference	v_{dc}^{*}	800 V
DC-link capacitor	C_{dc}	500 μF
Grid phase voltage amplitude	V_m	311 V
Filter inductance	L	5 mH
Filter resistance	R	0.1 Ω
Switching frequency	f_{sw}	20 kHz
Sampling frequency	$f_s = 1/T_s$	20 kHz

is to demonstrate the controller parameter design for the DC/AC power converter (i.e., the inverter), and thus it is assumed that the control of the boost converter is robust. That is, a constant power is fed to the DC-link.

In order to design the current controller analytically, Eq. (6.21) can be used with the parameters specified in Table 6.1. Accordingly, the PI control parameters for the d-axis current loop are obtained as

$$k_{pd} = 33.3 \quad \text{and} \quad k_{id} = 666.7 \tag{6.33}$$

where the bandwidth can be approximated using Eq. (6.23) as $f^{d}_{bw} = 1\,\text{kHz}$. Then, the DC-link voltage controller can be analytically designed on a basis of Eq. (6.32). In practice, the outer loop should be much slower than the inner current control loop in order to separate the cascaded control system [25]. With this consideration, the bandwidth of the outer DC-link voltage control loop should be limited between 1/50 and 1/10 of the current control loop. In this case study, a bandwidth of 100 Hz (i.e., 10 times slower than the inner current control loop) and then the PI parameters for the DC-link voltage are determined as

$$k_{pv} = 0.27 \quad \text{and} \quad k_{iv} = 16.11 \tag{6.34}$$

In order to verify the designed control parameters, the frequency responses of the open-loop and the closed-loop transfer functions of these control loops are plotted in Fig. 6.7. As it can be seen in Fig. 6.7A that a phase margin of 78.8° and 65.5° for the DC-link voltage control loop and the d-axis current control loop, respectively, is achieved with the designed parameters. The phase margins are sufficient to ensure the stability of the closed-loop control systems, as verified by Fig. 6.7B. However, as it is also shown in Fig. 6.7B, the bandwidth of the closed-loop d-axis current control (1.45 kHz) is higher than the approximated one (1 kHz) according to Eq. (6.23). Nevertheless, the outer

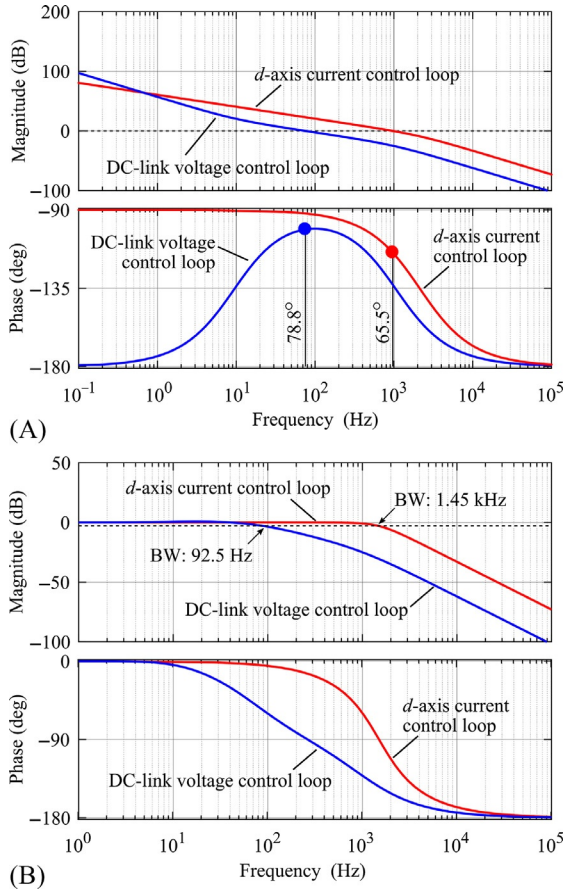

FIG. 6.7 Frequency response of the DC-link voltage and the *d*-axis current control loops with the designed parameters: (A) open loop Bode plots and (B) closed-loop Bode plots, where BW represents bandwidth of the system.

DC-link voltage control loop has a bandwidth of 92.5 Hz, which is much lower than the inner loop bandwidth. This guarantees that the inner loop can fully track the reference by the outer loop [25].

Furthermore, Fig. 6.8 shows the step response of these control loops. Clearly, as shown in Fig. 6.8 that the designed parameters for the DC/AC converter system ensure a much faster inner control loop. Therefore, the design is proper and the parameters can be used to control the double-stage DC/AC grid-connected converter system. This will be verified by the following simulation case in MATLAB.

Referring to Fig. 6.6, the designed controller parameters (i.e., Eqs. (6.33), (6.34)) are thus applied to a three-phase, grid-connected DC/AC power conversion system, and the model is built up in MATLAB. Simulation results are

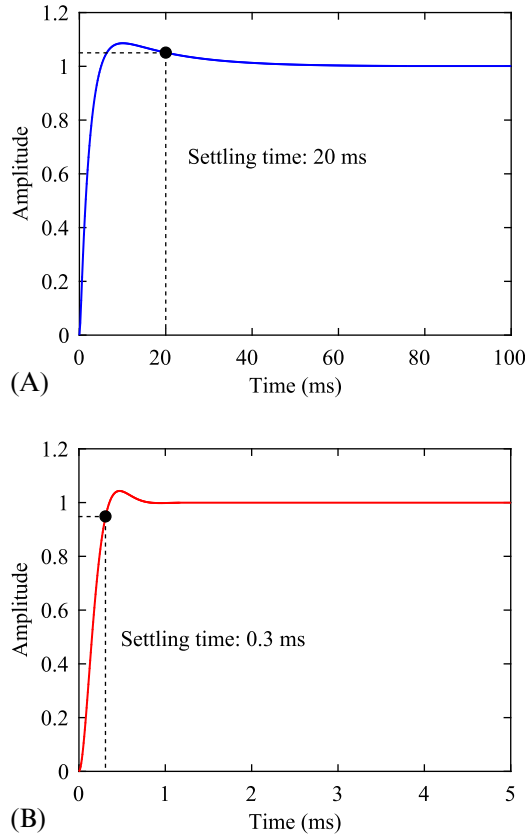

FIG. 6.8 Step responses of the closed-loop control systems for the DC/AC converter with the designed parameters: (A) the DC-link voltage control loop and (B) the *d*-axis current control loop.

reported in Fig. 6.9, in which the grid line-to-line voltages, grid line currents, DC-link voltage, and *dq*-current components are shown. In this case study, two transients have been employed, where the first transient is a step change in the active power from 0 to 8 kW, which is achieved through the boost converter control at $t = 0.2$ s; while the second one is a step change of the reactive power from 0 to 6 kVAR, which has been achieved through the *q*-current component at $t = 0.4$ s. As observed in Fig. 6.9, the designed controllers can follow the commands or references with high accuracy in the steady state. In the case of dynamic changes (i.e., at $t = 0.2$ s and $t = 0.4$ s), the control in the *dq*-reference frame enables the DC/AC system quickly to response to the disturbances. More specifically, when the input power is changed, the *d*-axis current will follow and react this change. This is also reflected at the DC-link, where the voltage presents an overshoot of about 7.5%, but it comes to steady state in one cycle. In contrast, the step change in the *q*-axis current is achieved by directly setting the

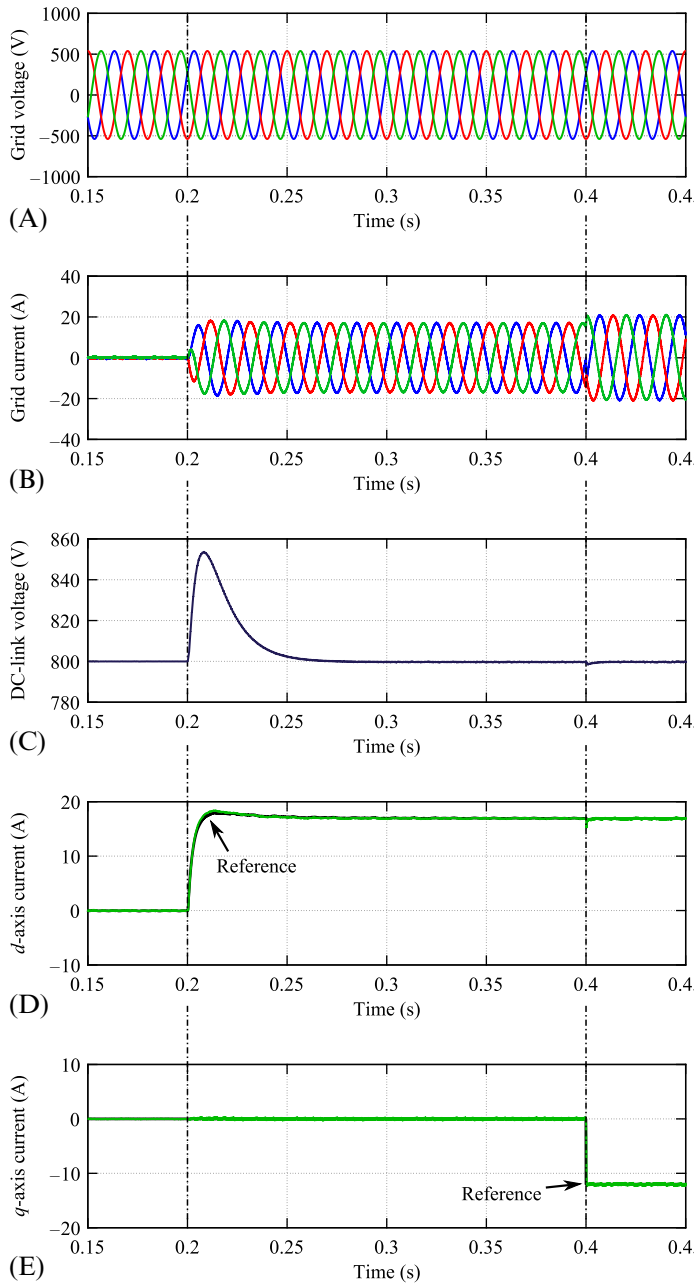

FIG. 6.9 Simulation results for the grid-connected three-phase AC/DC converter system controlled in the synchronous reference frame with the designed parameters: (A) grid line-to-line voltages, (B) grid currents, (C) DC-link voltage, (D) *d*-axis current component, and (E) *q*-axis current.

reactive power reference according to Fig. 6.6. Hence, there is a step-change in the q-axis current reference, which can be considered as a harsh operating condition in practice. Nevertheless, the designed PI controller for the q-axis current control loop can still quickly regulate the q-axis current with minor disturbances in the d-axis current, as shown in Fig. 6.9. In all, the designed controllers can properly control three-phase DC/AC converter with desired performances in terms of dynamics and control accuracy. Additionally, practical DC/AC converters may be connected to a weak grid with many low-order background harmonics and also to nonlinear loads (e.g., diode rectifiers). In that case, the currents injected to the load may be highly distorted with high harmonics. To improve the current quality, a harmonic compensation control should be implemented. This can also be done in either the dq-reference frame or the $\alpha\beta$-reference frame [15]. The audience of this book are advised to study this as an exercise to better understand the control of DC/AC converters.

The above has demonstrated the control of a three-phase DC/AC power converter, when connected to a grid. The design procedures presented in Sections 6.3.1 and 6.3.2 are validated by the case study. However, in practice, there are many applications employing single-phase full-bridge DC/AC power converters. As discussed previously, a fictitious system should be created in order to perform the Park transformations and then enable the application of PI controllers to regulate AC variables. If so, the presented controller design guidelines are still valid. Alternatively, the control can be achieved with proportional resonant (PR) controllers and repetitive controllers, which show high performance in tracking of AC variables [26,27]. In this case, the control loop can still be taken as a cascaded-control system. On the other hand, for grid-connected DC/AC converters, synchronization is mandatory, which is also a challenging issue, as discussed in Chapter 4. Typically, an orthogonal signal generator can be adopted for synchronization, which thus is beneficial to the control of single-phase DC/AC converters. That is, the design can be applied in single-phase grid-connected DC/AC converters without further efforts for creating the fictitious system that is in-quadrature with the original system.

In order to demonstrate this, an example of the current controller implemented with the PR controller in single-phase DC/AC converter will be shown in the following. The system and controller parameters are given in Table 6.2, while the controller parameters are designed following the discussion in Section 6.3, which gives

$$k_{pr} = 33.3 \quad \text{and} \quad k_{ir} = 13,334$$

The simulation results are shown in Fig. 6.10, where the reference output current experienced a step-change from 5 to 10 A at $t = 0.205$ s. The current responses of the single-phase DC/AC converter are transformed into the responses in the dq-reference frame, as shown in Fig. 6.10B. It can be seen from the results in Fig. 6.10 that the output current can follow the reference value,

TABLE 6.2 System Parameters of the 3.5-kW Grid-Connected Single-Phase DC/AC Converter

Parameter	Symbol	Value
DC-link voltage reference	v_{dc}^{*}	400 V
DC-link capacitor	C_{dc}	1000 μF
Grid phase voltage amplitude	V_m	230 V
Filter inductance	L	7.6 mH
Filter resistance	R	0.08 Ω
Switching frequency	f_{sw}	10 kHz
Sampling frequency	$f_s = 1/T_s$	10 kHz

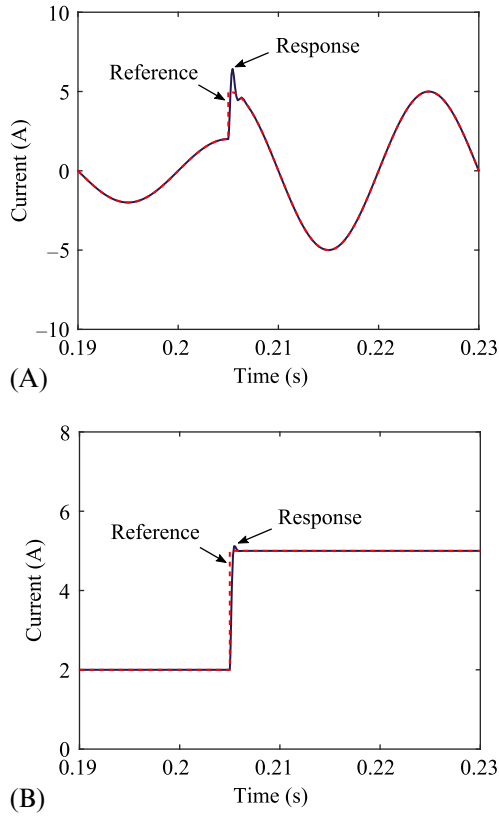

FIG. 6.10 Current step responses in single-phase DC/AC converters with the PR controller: (A) AC current (i.e., the α-axis current) and (B) the d-axis current.

ensuring the controllability of the current controller. However, as observed, the dynamics are slightly different in terms of overshoots and settling time. It is probably related to the coupling effects and the reference frame transformations in the control system. Nevertheless, this case study indicates that the control of single-phase DC/AC converters can be implemented in both the $\alpha\beta$-reference frame and the dq-reference frame.

6.4 SUMMARY

This chapter has presented the basic control of a three-phase two-level DC/AC power converters, where the detailed design of the PI controllers in the synchronous dq-reference frame was illustrated. First, the modeling of the three-phase DC/AC power converters was presented in terms of the current control loop in the dq-reference frame, the DC-link voltage, and the power control loop. The models enable the use of well-developed PI controllers to regulate the DC-voltage and the dq-axis currents for three-phase DC/AC converters, which have been demonstrated on a 10-kW three-phase grid-connected system. In respect to the control of single-phase DC/AC converters, similar modeling can be done, where a virtual system should be established in order to transform the AC control variables to DC quantities. A case study on a single-phase converter was demonstrated to show the controllability in the $\alpha\beta$-reference frame.

REFERENCES

[1] N. Mohan, T.M. Undeland, B. Robbins, Power Electronics, J. Wiley, New York, 1989.
[2] D.W. Novotny, T.A. Lipo, Vector Control and Dynamics of AC Machines, Clarendon Press, Oxford, 1996.
[3] B.K. Bose, Power electronics and motor drives recent progress and perspective, IEEE Trans. Ind. Electron. 56 (2) (2009) 581–588.
[4] F. Blaabjerg, Z. Chen, S.B. Kjaer, Power electronics as efficient interface in dispersed power generation systems, IEEE Trans. Power Electron. 19 (5) (2004) 1184–1194.
[5] R. Teodorescu, M. Liserre, P. Rodriguez, Grid Converters for Photovoltaic and Wind Power Systems, Wiley, New York, NY, USA, 2011.
[6] S.B. Kjaer, J.K. Pedersen, F. Blaabjerg, A review of single-phase grid-connected inverters for photovoltaic modules, IEEE Trans. Ind. Appl. 41 (5) (2005) 1292–1306.
[7] E. Romero-Cadaval, B. Francois, M. Malinowski, Q.C. Zhong, Grid-connected photovoltaic plants: an alternative energy source, replacing conventional sources, IEEE Ind. Electron. Mag. 9 (1) (2015) 18–32.
[8] IEEE Standard for Interconnecting Distributed Resources With Electric Power Systems, IEEE Std 1547-2003, 2003.
[9] European Network of Transmission System Operators for Electricity, Network code for requirements for grid connection applicable to all generators, Tech. Rep., 2013. Available: https://www.entsoe.eu.2013.

[10] Energinet.dk, Technical regulation 3.2.5 for wind power plants with a power output above 11 kW, Tech. Rep., 2010.
[11] Energinet.dk, Technical regulation 3.2.2 for PV power plants with a power output above 11 kW, Tech. Rep., 2015.
[12] Y. Yang, P. Enjeti, F. Blaabjerg, H. Wang, Wide-scale adoption of photovoltaic energy: grid code modifications are explored in the distribution grid, IEEE Ind. Appl. Mag. 21 (5) (2015) 21–31.
[13] Y.K. Wu, J.H. Lin, H.J. Lin, Standards and guidelines for grid-connected photovoltaic generation systems: a review and comparison, IEEE Trans. Ind. Appl. 53 (4) (2017) 3205–3216.
[14] R. Teodorescu, F. Blaabjerg, M. Liserre, P.C. Loh, Proportional-resonant controllers and filters for grid-connected voltage-source converters, IEE Proc. Electric Power Appl. 153 (5) (2006) 750–762.
[15] F. Blaabjerg, R. Teodorescu, M. Liserre, A.V. Timbus, Overview of control and grid synchronization for distributed power generation systems, IEEE Trans. Ind. Electron. 53 (5) (2006) 1398–1409.
[16] V. Blasko, V. Kaura, A new mathematical model and control of a three-phase AC-DC voltage source converter, IEEE Trans. Power Electron. 2 (1) (1997) 116–123.
[17] H. Akagi, Y. Kanazawa, A. Nabae, Instantaneous reactive power compensators comprising switching devices without energy storage components, IEEE Trans. Ind. Appl. IA-20 (3) (1984) 625–630.
[18] J. Kan, S. Xie, Y. Wu, Y. Tang, Z. Yao, R. Chen, Single-stage and boost-voltage grid-connected inverter for fuel-cell generation system, IEEE Trans. Ind. Electron. 62 (9) (2015) 5480–5490.
[19] A. Abdelhakim, P. Mattavelli, V. Boscaino, G. Lullo, Decoupled control scheme of grid-connected split-source inverters, IEEE Trans. Ind. Electron. 64 (8) (2017) 6202–6211.
[20] R. Teodorescu, F. Blaabjerg, M. Liserre, P.C. Loh, Proportional-resonant controllers and filters for grid-connected voltage-source converters, IEE Proc. Electric Power Appl. 153 (5) (2006) 750–762.
[21] P.C. Tan, P.C. Loh, D.G. Holmes, High performance harmonic extraction algorithm for a 25 kV traction power conditioner, IEE Proc. Electric Power Appl. 151 (2004) 505–512.
[22] D.G. Holmes, T.A. Lipo, B.P. McGrath, W.Y. Kong, Optimized design of stationary frame three phase AC current regulators, IEEE Trans. Power Electron. 24 (11) (2009) 2417–2426.
[23] C. Lascu, L. Asiminoaei, I. Boldea, F. Blaabjerg, High performance current controller for selective harmonic compensation in active power filters, IEEE Trans. Power Electron. 22 (5) (2007) 1826–1835.
[24] A.G. Yepes, F.D. Freijedo, Ó. Lopez, J. Doval-Gandoy, Analysis and design of resonant current controllers for voltage-source converters by means of Nyquist diagrams and sensitivity function, IEEE Trans. Ind. Electron. 58 (11) (2011) 5231–5250.
[25] D. Zhou, F. Blaabjerg, Bandwidth oriented proportional-integral controller design for back-to-back power converters in DFIG wind turbine system, IET Renew. Power Gener. 11 (7) (2017) 941–951.
[26] K. Zhou, D. Wang, Y. Yang, F. Blaabjerg, Periodic Control of Power Electronic Converters, IET Publisher, London, UK, 2016.
[27] Y. Yang, Advanced Control Strategies to Enable a More Wide-Scale Adoption of Single-Phase Photovoltaic Systems, Ph.D. Dissertation, Department of Energy Technology, Aalborg University, 2014. Available: http://vbn.aau.dk/ws/files/203989175/yongheng_yang.pdf.